First-principles analysis of solute diffusion in dilute bcc Fe-X alloys

Versteylen, Casper; van Dijk, Niels; Sluiter, Marcel

DOI
10.1103/PhysRevB.96.094105

Publication date
2017

Document Version
Final published version

Published in
Physical Review B (Condensed Matter and Materials Physics)

First-principles analysis of solute diffusion in dilute bcc Fe-*X* alloys

C. D. Versteylen,[1,2] N. H. van Dijk,[1] and M. H. F. Sluiter[2]

[1]*Fundamental Aspects of Materials and Energy, Faculty of Applied Sciences, Delft University of Technology, Mekelweg 15, 2629 JB Delft, The Netherlands*

[2]*Virtual Materials and Mechanics, Department of Materials Science and Engineering, Delft University of Technology, Mekelweg 2, 2628 CD Delft, The Netherlands*

(Received 22 June 2017; revised manuscript received 8 August 2017; published 7 September 2017)

The diffusivities of substitutional impurity elements in iron have been computed with *ab inito* electronic density functional techniques, using exchange-correlation functional PW91. Excess entropies and the attempt frequency for a jump were determined by calculating phonon frequencies in the harmonic approximation. The influence of the degree of spontaneous magnetization on diffusivity is taken into account by means of the Girifalco model. The activation energy for diffusion has been determined by computing the vacancy formation energy, impurity-vacancy binding energies, migration barrier energies, and the effective energy associated with correlation of vacancy-mediated jump. For each type of impurity atom these contributions have been evaluated and analyzed up to and including the fifth nearest-neighbor shell of the impurity atom. It is found that impurities that have a low migration energy tend to have high effective energy associated with vacancy migration correlation, and vice versa, so that the total diffusion activation energies for all impurities are surprisingly close to each other. The strong effect of vacancy migration correlation is found to be associated with the high migration energy for iron self-diffusion, so that movement of vacancies through the iron bulk is in all cases, except cobalt, the limiting factor for impurity diffusion. The diffusivities calculated with the PW91 functional show good agreement with most of the experimental data for a wide range of elements.

DOI: 10.1103/PhysRevB.96.094105

I. INTRODUCTION

Diffusional processes in metals are relevant for a wide variety of mechanisms, such as phase transformations and partitioning. In many cases the substitutional diffusivity is rate limiting for growth and coarsening of precipitate phases. Understanding and predicting such processes accurately requires knowledge of diffusivities of all elements present in a host. Here we present a systematic calculation of substitutional impurity diffusivities in bcc iron that makes it possible to compare the various contributing factors.

The diffusion of dilute substitutional impurities in iron has been the subject of many experimental studies [1–45]. It has become apparent that in contrast to impurity diffusion in, say, fcc aluminum, the diffusivities of subsitutional impurities in bcc iron do not differ very much from one another. However, a comprehensive comparison of *ab initio* computed substitutional diffusivity with actual experimental data, not just the fitted parameters, is highly desirable. This is particularly the case for diffusion in iron where an Arrhenius plot does not show a simple linear relation in the ferromagnetic state. Density functional theory (DFT) calculations have proven successful in predicting experimental data such as lattice parameters [46,47], elastic properties [48,49], and energy barriers for diffusion, e.g., diffusivities in aluminum [50], magnesium [51,52], and nickel [53]. Many impurity diffusivities in bcc iron [54–61] have been calculated with DFT methods, but oftentimes only experimentally fitted data, such as activation energy for diffusion, have been compared with the computed results. The fact that the Arrhenius plot of the diffusivity in bcc iron is not linear makes it desirable to compare the computed and experimentally determined diffusivities directly. This is because the determination of an activation energy for diffusion experimentally is not trivial because of the narrow temperature range available in the paramagnetic state.

The calculations were performed for the following elements (in the order of atomic number): Mg, Al, Si, P, S, Ca, Ti, V, Cr, Mn, Fe, Co, Ni, Cu, Zn, Ge, Zr, Nb, Mo, Ag, Sn, Sb, Hf, Ta, W, Au, Pb, and Bi. These elements were chosen to represent the entire periodic system of the elements and because of their use in the steel industry. In order to clarify trends, most elements of the fourth row, and of several columns, in the periodic table were considered. For 21 of these 28 diffusing elements the calculated results could be compared to experimental data. Some elements, such as the heavier alkaline-earth species and the rare earths proved to be so large in the iron matrix that a single-vacancy-assisted impurity diffusion mechanism was deemed unrealistic. We therefore excluded the elements Sr, Ba, Ce, and La from this study.

II. THEORY

Diffusivities in most metallic crystalline solids can be accurately described with an Arrhenius equation over a wide range of temperature with just two parameters, the activation energy for diffusion Q and the diffusivity prefactor D_0,

$$D = D_0 e^{-\beta Q}, \tag{1}$$

where $\beta = 1/(k_B T)$ with k_B the Boltzmann constant and T the absolute temperature. Accordingly, for most diffusivities, an Arrhenius plot gives a straight line, but for diffusion in bcc iron there is a systematic deviation from linearity near the Curie temperature. This deviation indicates the effect of magnetic order in the bcc iron matrix. Extensive experimental work [2–5,7,62] has resolved that around the Curie temperature the diffusivity prefactor is relatively little affected, but that

the activation energy for diffusion changes significantly. In analogy with CsCl type ordering on a bcc lattice, as occurs in β brass Cu-Zn alloys, Girifalco [63,64] derived a mean-field model to relate the magnetic order parameter to the diffusion activation energy,

$$Q = Q_{\mathrm{PM}}(1 + \alpha s^2), \tag{2}$$

where Q_{PM} is diffusion activation energy in the paramagnetic state (PM), α is a dimensionless proportionality constant, and s is the (dimensionless) magnetic order parameter in the ferromagnetic state (FM). The magnetic order parameter is given as a ratio of spontaneous magnetizations: $s = M(T)/M(T = 0)$, where $M(T)$ is the temperature-dependent spontaneous magnetization in the ferromagnetic state. In the perfectly ordered ferromagnetic state, with $s = 1$ the activation energy for diffusion Q_{FM} can be computed *ab initio*, so that Q_{PM} is obtained through

$$Q_{\mathrm{PM}} = \frac{Q_{\mathrm{FM}}}{1 + \alpha}. \tag{3}$$

The activation energy for substitutional diffusion in a pure metal includes a vacancy formation energy and a migration energy for the actual movement of the vacancy. As these energy terms are computed within finite-size supercells, rather than within a more or less infinitely large crystal, special care must be taken. To limit errors associated with wave expansions, calculations are performed in a supercell of constant (cubic) shape and volume. However, when a vacancy is introduced in such a cell, and/or when an iron atom is replaced by a large substitutional atom, under normal (practically zero external pressure) conditions, the supercell should relax to some other volume and/or shape. Therefore, we convert *ab initio* computed internal energies to zero pressure enthalpies according to

$$\begin{aligned} H[\text{supercell}] = {} & U[\text{supercell}] + P[\text{supercell}]V_0 \\ & + \tfrac{1}{2}U_{\mathrm{int}}[\text{supercell}], \end{aligned} \tag{4}$$

where P[supercell] is the hydrostatic pressure as computed *ab initio* within the fixed size supercell, and V_0 is the volume of the supercell. U_{int} is the elastic interaction between lattice defects due to periodic images that are unavoidable in supercell calculations. The energy correction has been computed using the program ANETO of Varvenne *et al.* [65], using the stiffness matrix parameters used to obtain the hydrostatic and dipole energies of all supercells. The stiffness matrix values are as follows: C_{11}, C_{22}, and C_{33}: 268.760 GPa; C_{12}, C_{21}, C_{13}, C_{31}, C_{32}, and C_{23}: 154.450 GPa; and C_{44}, C_{55}, and C_{66}: 89.400 GPa. We used supercells consisting of $4 \times 4 \times 4$ bcc cubes with a lattice parameter of $a = 0.283$ nm, giving $V_0 \approx 1.45$ nm^3. We selected $a = 0.283$ nm because it is the zero pressure value for pure bcc iron according to the PW91 generalized gradient approximation (GGA) exchange-correlation potential (xc potential). At $T = 0$ K, the vacancy formation enthalpy can then be computed with

$$\Delta H_{f,\square} = H[\mathrm{Fe}_{N-1}\square] - \frac{N-1}{N}H[\mathrm{Fe}_N], \tag{5}$$

where $Fe_{N-1}\square$ refers to a supercell with $N - 1$ iron atoms and a single vacancy, where $N = 128$ for a $4 \times 4 \times 4$ supercell.

Of course, the effect of a vacancy or impurity atom is not limited to the ground-state properties, as excitations are also affected. Therefore, the formation free energy of a defect is evaluated by adding the free-energy contribution due to excitations to defect formation enthalpy. In the case of a vacancy this gives

$$\Delta G_{f,\square}(T) = \Delta H_{f,\square} + \Delta\Delta G_{\mathrm{exc},\square}(T), \tag{6}$$

where $\Delta\Delta G_{\mathrm{exc},\square}(T)$ is the free-energy change associated with a defect (here a vacancy) due to excitations, such as related to electrons and phonons. Calculations in supercells with and without a defect give

$$\begin{aligned} \Delta\Delta G_{\mathrm{exc},\square}(T) = {} & \Delta G_{\mathrm{exc}}(T)[\mathrm{Fe}_{N-1}\square] \\ & - \frac{N-1}{N}\Delta G_{\mathrm{exc}}(T)[\mathrm{Fe}_N], \end{aligned} \tag{7}$$

analogous with Eq. (5). The electronic excitations are evaluated by varying the electron temperature in the Fermi-Dirac distribution function in the supercell calculations. Vibrational excitations have been evaluated in the harmonic approximation using zone-centered supercell modes. Then, the vibrational free energy G_{vib} is computed from the phonon frequencies ω_i using [66]

$$\Delta G_{\mathrm{vib}}(T) = \sum_i \frac{1}{2}\hbar\omega_i + k_B T \ln(1 - e^{-\beta\hbar\omega_i}). \tag{8}$$

At high temperatures the excess vibrational free energy associated with a defect is approximately linear with temperature, $\lim_{T\to\infty} \Delta G_{\mathrm{vib}}(T) = T\sum_i k_B \ln(\hbar\omega_i)$. The excess vibrational enthalpy difference behaves as the reciprocal of temperature and therefore vanishes. The vibrational formation energy of a vacancy is obtained through

$$\Delta\Delta G_{\mathrm{vib},\square}(T) \approx \Delta\Delta H_{\mathrm{vib},\square} - T\Delta\Delta S_{\mathrm{vib},\square}, \tag{9}$$

where, in the high-temperature limit, $\Delta\Delta H_{\mathrm{vib},\square} = 0$ and the effective vacancy formation entropy arises from the difference between the ΔS contributions of a cell with and without a vacancy;

$$\begin{aligned} \Delta\Delta S_{\mathrm{vib},\square} = {} & -\sum_i k_B \ln(\hbar\omega_i[\mathrm{Fe}_{127}\square]) \\ & + \frac{127}{128}\sum_i k_B \ln(\hbar\omega_i[\mathrm{Fe}_{128}]). \end{aligned} \tag{10}$$

Specific to bcc iron is a correction for the diffusivity activation energy in order to capture the effect of magnetism [64] [see Eq. (2)] through the relative spontaneous magnetization s. The temperature dependence of s is accurately represented by an empirical formula [67],

$$s(\tau) = \frac{(1-\tau)^B}{1 - B\tau + A\tau^{3/2} - C\tau^{7/2}}, \tag{11}$$

where τ is the reduced temperature ($\tau = \frac{T}{T_C}$), with the Curie temperature $T_C = 1043$ K in bcc iron. The constants take the values [67] $A = 0.11$, $B = 0.368$, and $C = 0.129$. The parameter α, which indicates how much the magnetic disordering affects the activation barrier for diffusion, was found to be similar for all solute elements in bcc iron. The determination of this parameter is discussed by the authors in a

separate paper [68]. The parameter $\alpha = 0.10$ for all impurities in Fe, except for iron self-diffusion where $\alpha = 0.16$.

A. Self-diffusion

To determine the self-diffusivity D[Fe], the migration energy for the movement of a vacancy to a neighboring iron atom needs to be calculated. The migration energy ΔH_{mig} is the energy difference between energies of the transition state (tr) and equilibrium state (eq). The rate Γ at which a vacancy trades place with its neighbor atom can then be expressed as

$$\Gamma = \nu e^{-\beta \Delta H_{\text{mig}}}, \tag{12}$$

where ν is the attempt frequency and where the exponential gives the probability of success. In the transition state the evaluation of the vibrational excitations requires care because of the negative curvature of the energy along the transition path. Therefore, the vibrational contribution to the migration free energy is treated according to transition-state theory [69]. The effective jump attempt frequency $\tilde{\nu}$ is given by [69]

$$\tilde{\nu} = \frac{\prod \nu_i[\text{eq}]}{\prod' \nu_i[\text{tr}]}, \tag{13}$$

where the product of vibrational modes ($\prod \nu_i$) of a system with a vacancy is computed with a diffusing atom in the transition state ([tr]) and with all atoms in the equilibrium state ([eq]). The imaginary frequency representing the direction of the unstable vibrational mode of the transition state is specifically excluded from the product, as is indicated by the prime in the product operator in the denominator. In our calculations, we ignore the effect of thermal lattice expansion, and the small contribution of the electronic excitations is neglected also. The vacancy migration rate is then

$$\Gamma = \tilde{\nu} e^{-\beta \Delta H_{\text{mig}}}, \tag{14}$$

where $\tilde{\nu}$ is given by Eq. (13), and ΔH_{mig} is computed with

$$\Delta H_{\text{mig}} = H_{tr}[\text{Fe}_{N-1}\square] - H_{eq}[\text{Fe}_{N-1}\square], \tag{15}$$

where $H_{tr}[\text{Fe}_{N-1}\square]$ is the enthalpy of a supercell in the transition state (the saddle-point configuration where an atom is about midway its jump) and $H_{eq}[\text{Fe}_{N-1}\square]$ concerns the situation prior to the jump where all atoms are still in their equilibrium positions.

The self-diffusivity D[Fe] is the product of the migration rate Γ, the vacancy concentration $C_\square$, a correlation factor f, and the actual jump distance l that a migrating atom travels squared,

$$D[\text{Fe}] = C_\square l^2 f \Gamma. \tag{16}$$

The jump distance is equal to the nearest-neighbor distance $l = \frac{\sqrt{3}}{2} a$ in the case of bcc iron, where a is the bcc lattice parameter of iron. The correlation factor f describes how efficiently the vacancy contributes to the movement of iron atoms. It can be calculated with the nine-frequency model of Le Claire [70,71], which yields a constant value $f = 0.727$ in the case of self-diffusion in bcc.

The vacancy concentration is assumed to be at equilibrium in the low-concentration limit and therefore given by an Arrhenius equation with prefactor unity and with the Gibbs energy of vacancy formation $\Delta G_{f,\square}$ as

$$C_\square = e^{-\beta \Delta G_{f,\square}}, \tag{17}$$

where $\Delta G_{f,\square}$ is given by Eq. (6).

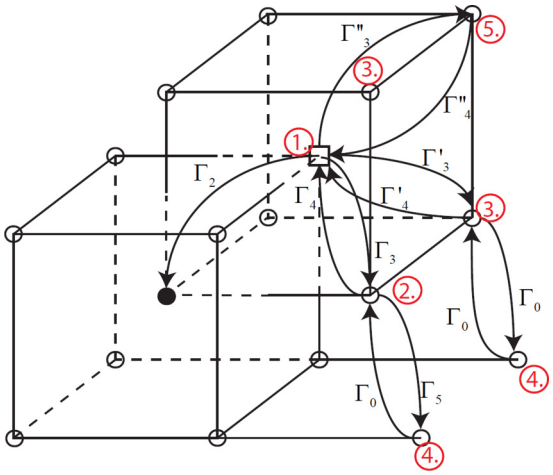

FIG. 1. The nine-frequency model by Le Claire [70,71]. Each distinct jump frequency is indicated, with the red numbers indicating the nearest neighbor with respect to the impurity atom. Γ_2 concerns the impurity trading places with the vacancy, Γ_3 concerns an iron atom that is a second neighbor of the impurity exchanging with a vacancy and thereby becoming a nearest neighbor to the impurity, Γ_4 is the reverse of Γ_3, $\Gamma_{3'}$ is a jump whereby an iron atom changes from a first to a third neighbor of the impurity, $\Gamma_{4'}$ is the reverse of $\Gamma_{3'}$, an iron atom jumping from first to fifth impurity neighbor is $\Gamma_{3''}$, and $\Gamma_{4''}$ is the reverse of $\Gamma_{3''}$. All other jump frequencies are assumed to be unaffected by the presence of a substitutional solute and are assumed to take the same value as the one in pure iron bulk Γ_0.

B. Impurity diffusion

In comparison with self-diffusion, impurity diffusion introduces several new factors because of the interaction between the impurity atom and the vacancy. One can recognize the influence of the two point defects (a) on the correlation factor because of a variety of migration barriers and (b) on vacancy binding at various distances from the impurity both as a binding enthalpy and as a binding entropy. First we consider how a vacancy moves in the immediate vicinity of a substitutional diffusing species via the correlation factor. Unlike in the case of self-diffusion, there are multiple jump rates because after a jump the vacancy can have a new position relative to the impurity atom, as is illustrated in Fig. 1. Each of the distinct jumps has its own migration enthalpy and its own jump rate. Of course, the migration enthalpy is generally not the same in both directions. We will assume that the jump attempt frequency, $\tilde{\nu}$ in Eq. (14), takes the value of pure iron for all jumps of iron atoms given by Eq. (13). For the Γ_2 jump, where an X impurity atom jumps, we compute the jump rate according to Eq. (13). Details concerning the attempt frequency are generally not extremely important because it varies over a relatively small range of values compared to the Boltzmann factor which varies over many orders of magnitude as a function of temperature.

The correlation factor f of an impurity diffusing in a bcc system was approximated by Le Claire [70,71] with a model

explicitly considering nine distinct jump rates Γ, the so-called nine-frequency model,

$$f = \frac{3\Gamma_3+3\Gamma_{3'}+\Gamma_{3''}-\frac{\Gamma_3\Gamma_4}{\Gamma_4+F\Gamma_5}-\frac{2\Gamma_{3'}\Gamma_{4'}}{\Gamma_{4'}+3F\Gamma_0}-\frac{\Gamma_{3''}\Gamma_{4''}}{\Gamma_{4''}+7F\Gamma_0}}{2\Gamma_2+3\Gamma_3+3\Gamma_{3'}+\Gamma_{3''}-\frac{\Gamma_3\Gamma_4}{\Gamma_4+F\Gamma_5}-\frac{2\Gamma_{3'}\Gamma_{4'}}{\Gamma_{4'}+3F\Gamma_0}-\frac{\Gamma_{3''}\Gamma_{4''}}{\Gamma_{4''}+7F\Gamma_0}}, \tag{18}$$

with the factor $F = 0.512$.

The correlation factor f, Eq. (18), depends on temperature because each of the Γ varies with temperature [Eq. (14)]. The influence of temperature on the correlation factor can be quite significant for elements with large variations in $\Delta H_{\mathrm{mig},i}$. In spite of the complex formal temperature dependence of the correlation factor, usually it is well approximated by a simple Arrhenius equation because one of the jump frequencies Γ_i tends to become the bottleneck in the diffusive process. A simple analysis of Eq. (18) shows that the numerator is dominated by the largest terms; either Γ_3, $\Gamma_{3'}$, or $\Gamma_{3''}$. If the largest Γ in the numerator is larger than Γ_2 in the denominator, f will be approximately unity almost independent of temperature. However, if Γ_2 is larger than the largest Γ in the numerator, their ratio will be a good estimate of f,

$$f \approx \frac{\max(\Gamma_3,\Gamma_{3'},\Gamma_{3''})}{\max(\Gamma_2,\Gamma_3,\Gamma_{3'},\Gamma_{3''})}. \tag{19}$$

The jump rates are all Boltzmann factors, so that f is approximated by an Arrhenius equation. This leads to the definition of an effective entropy and effective enthalpy of correlation by fitting a linear relation between $\ln(f)$ and β,

$$\ln(f) \sim \Delta S_c/k_B - \beta\Delta H_c. \tag{20}$$

The approximation for f in Eq. (19) then yields for $\Delta H_c \approx \max[0, \min(\Delta H_{\mathrm{mig},3}, \Delta H_{\mathrm{mig},3'}, \Delta H_{\mathrm{mig},3''}) - \Delta H_{\mathrm{mig},2}]$. When fitting within the temperature range between 600 and 1200 K and accounting for the negative terms in the numerator and denominator in Eq. (18), it is found that a minor rescaling is required which gives

$$\Delta H_{c,\mathrm{approx}} = 1.2\ \max[0, \min(\Delta H_{\mathrm{mig},3}, \Delta H_{\mathrm{mig},3'}, \Delta H_{\mathrm{mig},3''}) - \Delta H_{\mathrm{mig},2}]. \tag{21}$$

The effective entropy of correlation is not easily estimated by an approximate expression.

The impurity-vacancy binding at various separation distances is temperature dependent and thus can be thought of as both a binding enthalpy and as a binding entropy. The enthalpy differences at zero pressure are evaluated with

$$\Delta H_{\mathrm{bind},X\square}(\mathbf{R}_j) = H[\mathrm{Fe}_{N-2}X\square](\mathbf{R}_j) - H[\mathrm{Fe}_{N-1}X] - H[\mathrm{Fe}_{N-1}\square] + H[\mathrm{Fe}_N], \tag{22}$$

where each of the supercell enthalpies have been computed using Eq. (4), and where $\mathbf{R}_j$ indicates the shortest vector that separates X and $\square$. The entropic binding terms then arise from electronic, magnetic, and vibrational excitations. The electronic excitations are easily incorporated self-consistently through the Fermi-Dirac distribution function. We find these effects to be negligible. The magnetic excitations are globally included through the Girifalco model. Of course, magnetic behavior, and its temperature dependence, must be expected to differ from the global pure Fe bulk in the vicinity of a defect. We have chosen to neglect such local defect-induced excess terms. The excess vibrational free energy associated with vacancy-impurity binding has been calculated from supercells with and without defects, analogous to Eq. (10).

$$\begin{aligned}\Delta\Delta S_{\mathrm{bind},X\square}(\mathbf{R}_j) &= -\sum_i k_B \ln(\hbar\omega_i[\mathrm{Fe}_{N-2,X,\square}]) + \sum_i k_B \ln(\hbar\omega_i[\mathrm{Fe}_{N-1,X}]) \\ &\quad + \sum_i k_B \ln(\hbar\omega_i[\mathrm{Fe}_{N-1,\square}]) - \sum_i k_B \ln(\hbar\omega_i[\mathrm{Fe}_N]).\end{aligned} \tag{23}$$

As indicated in Eq. (9), the excess vibrational free energy can be separated in a vanishing excess vibrational enthalpy $\Delta H_{\mathrm{vib},X\square}(\mathbf{R}_j)$ and an approximately temperature-independent vibrational impurity-vacancy binding entropy $\Delta S_{\mathrm{vib},X,\square}(\mathbf{R}_j)$ term. The activation barrier for diffusion in the fully ferromagnetically ordered state is calculated as the sum of the various contributions,

$$Q_{\mathrm{FM}} = \Delta H_{f,\square} + \Delta H_{\mathrm{bind},X\square}(\mathbf{R}_1) + \Delta H_{\mathrm{mig},2} + \Delta H_c, \tag{24}$$

where $\mathbf{R}_1$ indicates a nearest neighbor in the bcc crystal structure. The paramagnetic activation energy for diffusion is computed from Q_{FM} with Eq. (3). The preexponential factor D_0 in Eq. (1) is calculated in the purely ferromagnetic state and is assumed to be the same for PM and FM states. This is justified by the relatively small shifts in phonon shift frequencies [72–74]. In addition, the shift in phonon frequencies is gradual with temperature [75,76]. The entropy contribution which originates from the correlation is modest and the difference with magnetic order is expected to be small as well.

$$D_0 = \tfrac{3}{4}a^2\tilde{\nu}_2 e^{(\Delta\Delta S_{\mathrm{vib},\square}+\Delta\Delta S_{\mathrm{bind},X\square}(\mathbf{R}_1)+\Delta S_c)/k_B}, \tag{25}$$

where $\Delta\Delta S_{\mathrm{vib},\square}/k_B$ applies to pure iron.

III. FIRST-PRINCIPLES CALCULATIONS

Enthalpies (total energies) have been computed within the local density approximation using the Vienna *ab initio* simulation program (VASP) [77,78] version 5.2 at a pressure of 0 GPa. The calculations were performed using pseudopotentials of the projector augmented wave type [79]. Standard potentials were used [80], except for atoms much larger than Fe where harder potentials with semicore states treated as valence states were used: Bi_d, Ca_pv, Ge_d, Hf_pv, Mo_pv, Nb_pv, Pb_d, Sn_d, Ta_pv, Ti_pv, V_pv, W_pv, and Zr_sv. Supercells with $4 \times 4 \times 4$ conventional bcc cubes (128 lattice sites) were employed, with $5 \times 5 \times 5$ Γ-centered k-point grids in the case of the vacancy formation energies and migration barriers with an energy cutoff of 400 eV for plane-wave expansions. For the vacancy-impurity binding phonon calculations the cutoff frequency was chosen to be 440 eV, in $3 \times 3 \times 3$ bcc supercells with $4 \times 4 \times 4$ Γ-centered k-point grids. All calculations were spin-polarized. Migration barriers have been calculated with the nudged-elastic band (NEB) method with the climbing image algorithm [81]. Elastic energy corrections for image interactions associated with supercells were made

TABLE I. Calculated vacancy formation enthalpies ($\Delta H_{f,\square}$) calculated with Eq. (5), and entropies ($\Delta\Delta S_{\text{vib},\square}$) calculated with Eqs. (5) and (10), comparison of various xc functionals.

xc type	$\Delta H_{f,\square}$ (eV)	$\Delta\Delta S_{\text{vib},\square}$ (k_B)
PW91	2.129 (this work)	4.14 (this work)
PW91	2.02 [56]	
PW91	2.0 [104]	
PW91	2.16 [88]	
PW91	2.16 [46]	
PW91	2.16 [94]	4.08 [94]
PBE	2.18 [105]	4.62 [105]
PBE	2.13 [87]	
PBE	2.23 [57]	
PBE	2.01 [89]	
PBE	2.22 [46]	
PBE	2.31 [90]	
PBEsol	2.626 (this work)	
PBEsol	2.47 [46]	
revTPSS	2.64 [46]	

using the method of Varvenne *et al.* [65]. The elastic interaction energy is computed from the pressure and the deviatoric stress computed *ab initio* within supercells with fixed volume and fixed (cubic) shape. Elastic energy corrections for image interactions were typically in the order of meVs at most for the $4 \times 4 \times 4$ supercells, with the larger values occurring for the transition-state configurations. In our calculations two GGA xcfunctionals were used: PW91 [82,83] and PBEsol [84]. The PBEsol xc functional was designed with the aim to correct for an inaccuracy in predicted lattice constants of PW91 and PBE. The overestimation of lattice parameters [in the case of Perdew-Burke-Ernzerhof (PBE)] coincides with an underestimation of the bulk modulus of pure metals; PBEsol is reported to give a better approximation for many different pure metals [47]. However, PBEsol for bcc iron fails at predicting the lattice parameter, giving 2.79 Å [85], to be compared with an experimental value of about 2.86 Å. At the theoretical lattice parameter (2.79 Å), PBEsol gives a rather high vacancy formation enthalpy [46,86], about 2.47 eV, which is beyond the current generally accepted value of about 2.2 eV [46,57,87–90]. The results of the PBEsol calculated energies are therefore presented only in Table I and in the Supplemental Material [91]. The PBEsol computed value increases to even higher values when a more realistic value for the lattice parameter is selected [46]. At the bcc lattice parameter selected in this work—2.83 Å, the PW91 equilibrium value—it is to be expected that too large a vacancy formation enthalpy is computed for PBEsol. However, recent work by Glensk *et al.* [92] has called into question the validity of currently generally accepted vacancy formation enthalpies, so that we find it of interest to consider the PBEsol functional.

IV. RESULTS AND DISCUSSION

A. Vacancy formation and impurity-vacancy binding enthalpy

The vacancy formation enthalpy in pure bcc iron was computed with Eq. (5) (see Table I). Table I shows that there is agreement with previously published data. Our PW91 vacancy formation enthalpy is in the middle of the range of values

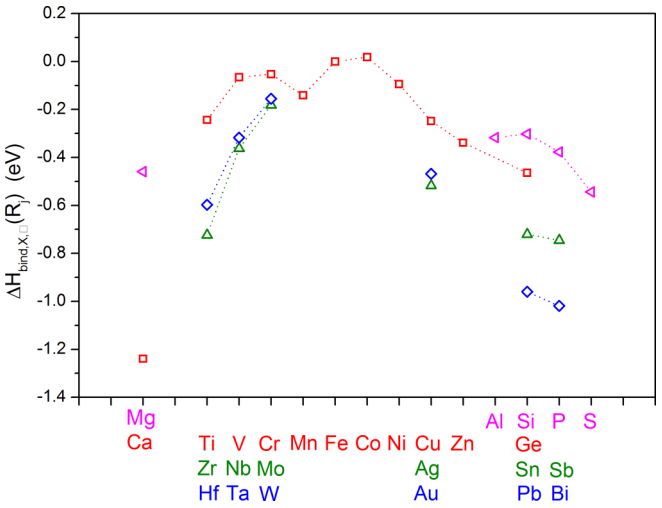

FIG. 2. Vacancy binding enthalpy next to a single impurity atom as computed with 22 using PW91. Impurity elements are arranged by row and column of the periodic system: row 3 of the periodic system (purple triangles), row 4 of the periodic system (red squares), row 5 of the periodic system (green triangles), and row 6 of the periodic system (blue diamonds). Dashed lines, between neighboring impurities, are guides to the eyes only.

reported in the literature and it agrees nicely also with results published for the PBE GGA [93]. PBEsol rather consistently gives values almost half an eV higher than PW91 and PBE.

The vacancy formation vibrational entropy [see Eq. (9)] in bcc iron is computed to be about $4.14k_B$ for PW91 in a $4 \times 4 \times 4$ supercell. This value is in good agreement with the value obtained by Lucas and Schäublin [94], $\Delta\Delta S_{\text{vib},\square} = 4.08k_B$, and a little less close agreement with the value by Messina *et al.* [61], $\Delta\Delta S_{\text{vib},\square} = 4.6k_B$. The vacancy formation vibrational entropy obtained in a $3 \times 3 \times 3$ supercell is $3.79k_B$, quite close to our $4 \times 4 \times 4$ result. In view of the computational resources needed, and the relatively small effect on the diffusivity, we use the $4 \times 4 \times 4$ result for the vacancy formation vibrational entropy, and the $3 \times 3 \times 3$ supercell results for the vacancy-impurity binding entropy. The vacancy formation vibrational entropy is quite large in comparison to other single site excess entropies: the configurational entropy in real alloys and entropy differences between allotropes are usually in the neighborhood of $1k_B$ or less [95].

The impurity-vacancy binding enthalpies, computed with Eq. (22), are plotted in Fig. 2. These enthalpies correlate well with the columnar position in the periodic table of the elements of the impurity atom. The row position of the impurity atom is less discriminating; for elements in the same column, row 5 and row 6, differ little from one another. There is a minimum at the edges of the periodic system of the transition metals in each row of the periodic table. Of course, atoms at the middle of the transition-metal series are usually smallest confirming a well-documented relation to atomic sizes [50,51]. There have been several studies of vacancy-impurity binding in bcc iron [57–59,61,96,97] and our results mostly agree with previous calculations with a few notable exceptions: For cobalt our results, and those of Olsson *et al.* [97] and Messina *et al.* [61], are in marked contrast to those of Ohnuma *et al.* [96]. For

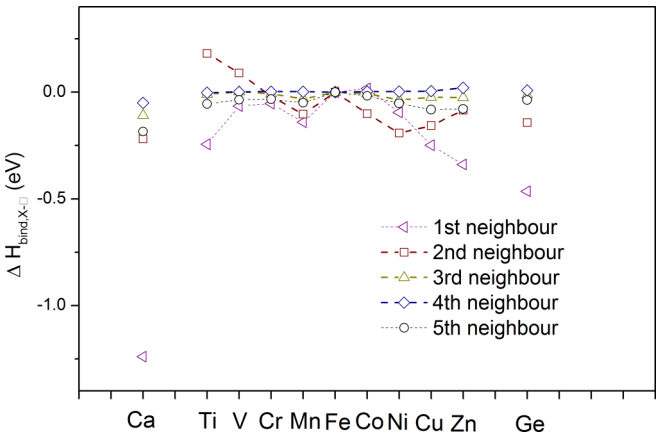

FIG. 3. Vacancy-impurity enthalpy for impurities in the fourth row of the periodic table as computed with Eq. (22) using PW91. Nearest neighbors: purple triangles; second neighbors: burgundy squares; third neighbors: green triangles; fourth neighbors: blue diamonds; fifth neighbors: black circles.

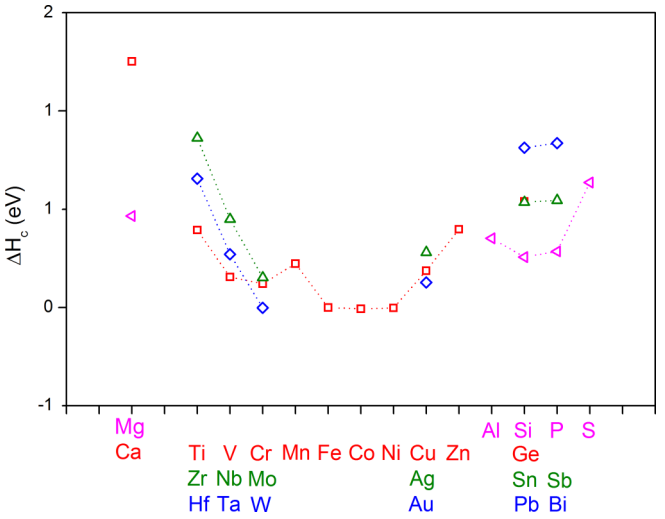

FIG. 4. Effective enthalpy of correlation calculated with Eq. (20) derived from the temperature relation of correlation factors of impurity elements, arranged by row and column of the periodic system: row 3 of the periodic system (purple triangles), row 4 of the periodic system (red squares), row 5 of the periodic system (green triangles), and row 6 of the periodic system (blue diamonds). Dashed lines, between neighboring impurities, are guides to the eyes only.

nickel we agree with Refs. [61,97], but disagree with those of Vincent *et al.* [58]. For copper our results are closest to those of Ohnuma *et al.* [96], and close to those of Refs. [61,97], but differ significantly from others [58,59]. For Mo we agree with Huang *et al.* [57] and Refs. [61,97], but not with Ohnuma *et al.* [96]. For some elements we did not find literature values to compare with Bi, Ca, Ge, Mg, Pb, and Sn. Details for the impurity-vacancy binding up to the fifth shell for all impurities can be found in the Supplemental Material [91].

The vacancy-impurity binding enthalpy varies rather systematically with distance as can be seen in Fig. 3 and was also reported by others [61,97]: relative to the binding at the first nearest neighbor, the second neighbor binding is a bit weaker, at the third and fourth neighbors the binding is much weaker, while at the fifth neighbor, it is again stronger, but weaker than at the first and second neighbors. This can be rationalized by the strong transmission of strain effects along a dense packed direction, such as applies to the first and fifth neighbors.

B. Migration barriers

The migration enthalpies of various impurity elements in iron and the barriers of the iron atoms in the vicinity of the impurity were computed with Eq. (15). Large impurity atoms, such as toward the left and right extremities of the periodic table, have low values for $\Delta H_{\mathrm{mig},2}$ (see Fig. 4). Impurities close to Fe in the middle of the periodic table have $\Delta H_{\mathrm{mig},2}$ of similar magnitude as ΔH_{mig} for iron self-diffusion with the exception of Mn, which has a much lower barrier. This trend was reported by Ding *et al.* [60] and Messina *et al.* [61] also. It has been found for transition-metal (TM) impurities diffusion in fcc Ni as well [53]. The inverse relation between the magnitude of $\Delta H_{\mathrm{mig},2}$ and atomic size has been rationalized through the displacement of the large impurity atom toward the vacancy. This results in short jump distances and correspondingly low barriers [50]. Very large impurity atoms such as Sr, Ba, Ce, and La take an intermediary position between the original position and the neighboring vacancy, forming a vacancy-impurity atom complex. Such complexes can probably only migrate when an additional vacancy approaches. Such double-vacancy-assisted diffusion processes have not been explored in the current work. For calcium a nearest-neighbor jump, although shortened, still can be defined, but the associated migration enthalpy is 19 meV only. In such a case the Ca atom frequently jumps back and forth without any net displacement, and diffusion of the calcium atom is going to be determined by how the vacancy migrates through the neighboring bulk, that is, it will be determined by the correlation factor, as will be discussed below.

Large impurity atoms, at the left and right sides of the periodic table, generally have strong vacancy binding (see Fig. 2). As a result their migration barriers for dissociative jumps $\Delta H_{\mathrm{mig},3}$, $\Delta H_{\mathrm{mig},3'}$, and $\Delta H_{\mathrm{mig},3''}$ tend to be much larger than the corresponding barriers for associative jumps $\Delta H_{\mathrm{mig},4}$, $\Delta H_{\mathrm{mig},4'}$, and $\Delta H_{\mathrm{mig},4''}$. For many larger atoms $\Delta H_{\mathrm{mig},4''}$ is the lowest barrier (Ca, Zr, S, Hf, Pb, Bi, Ge, P, Sn, Mn, Sb, Si, Cu, Cr, Au, and W), whereas for others (Mg, Nb, Ti, Zn, Ag, Al, Ta, V, and Mo) it is $\Delta H_{\mathrm{mig},4'}$. For Co and Ni only, we find $\Delta H_{\mathrm{mig},3}$ to be the lowest barrier. Not surprisingly Ni has almost no vacancy binding, and Co is the only element (in our analysis) that we found that repels a vacancy at the nearest-neighbor shell in bcc Fe.

The migration enthalpies for all the impurity species form a large data set. Therefore, all detailed information concerning migration enthalpies is tabulated in Table III of the Supplemental Material [91], with a detailed comparison to literature data.

C. Correlation factor

Using Eq. (18), the correlation factor for each impurity species has been computed as a function of temperature. As

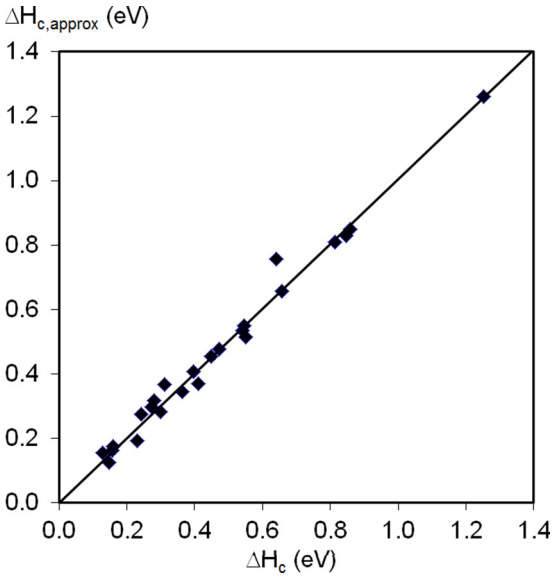

FIG. 5. Effective enthalpy associated with correlation as estimated from Eq. (21), ΔH_c[approx] as a function of the ΔH_c obtained from Eq. (20) within the temperature range of 600–1200 K for all elements considered in this study. The most overestimated value pertains to sulfur.

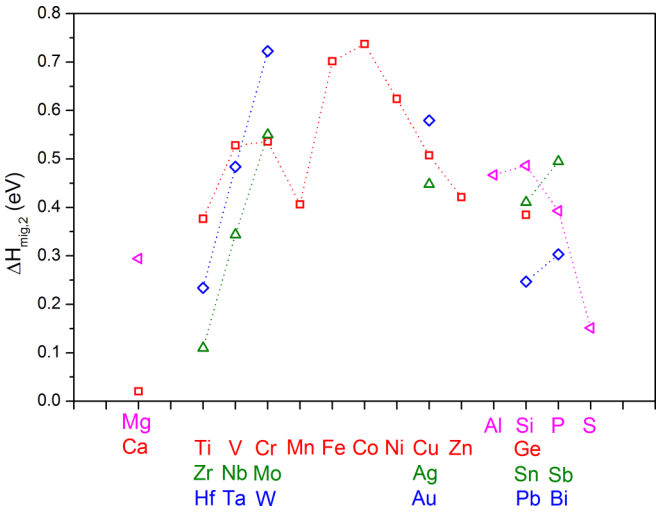

FIG. 6. Migration enthalpy $\Delta H_{\mathrm{mig},2}$ of impurity elements calculated with Eq. (15), arranged by row and column of the periodic table: row 3 of the periodic system (purple triangles), row 4 of the periodic system (red squares), row 5 of the periodic system (green triangles), and row 6 of the periodic system (blue diamonds). Dashed lines, between neighboring impurities, are guides to the eyes only.

the correlation factor is found to be described rather well by an Arrhenius relation, an effective entropy and effective enthalpy of correlation has been defined [Eq. (20)]. ΔH_c is significant for several impurity species, especially for impurity species at the far left and far right of the periodic table (see Fig. 7). This result relates with the finding that large impurity atoms diffusing in a Mg matrix also feature significant effective correlation enthalpies [51,52]. However, position in the periodic table gives a more significant correlation than atomic size. Tungsten and gold are larger atoms than chromium and copper, but the latter two have larger effective correlation enthalpies. Likewise sulfur, phosphorous, and germanium have much larger effective correlation enthalpies than their atomic size in the bcc Fe matrix would suggest, but they are clearly far to the right from Fe in the periodic table. For elements with large ΔH_c one cannot neglect the temperature dependence of the correlation factor, as has been found in Mg also [51,52].

An analysis of the expression for the correlation factor has revealed that an approximate analytic expression can be derived [see Eq. (21)]. In Fig. 5 the accuracy of the approximate expression can be gauged. The approximation deviates typically by up to about 5% of the value obtained by fitting according to Eq. (20) with f from Eq. (18). Equation (21) also suggests a negative correlation between ΔH_c and $\Delta H_{\mathrm{mig},2}$. This is confirmed by the opposite tendencies in Figs. 4 and 7. When ΔH_c is plotted as a function of $\Delta H_{\mathrm{mig},2}$, in Fig. 6, this negative correlation is evident.

Clearly, when the activation energy of diffusion is computed, using Eq. (24), two element-specific terms, ΔH_c and $\Delta H_{\mathrm{mig},2}$, have the tendency to compensate one another. As a result, the activation energy of impurity diffusion in bcc Fe does not vary nearly as much as in some other metallic matrices (e.g., fcc Al [50]). It is clear that the temperature dependence of the correlation factor should not be ignored, in contrast to some previous studies [54,57,60,88]. Fortunately for elements close to iron in the periodic table ΔH_c is relatively small (see Fig. 7). Evaluating the correlation factor at one specific temperature [98] is thus likely to give a large error in the calculated diffusion activation energy of yttrium, titanium, and zirconium.

The effective entropy associated with correlation as obtained by fitting to Eq. (20) within $T = 600$–1200 K is much less transparent. For Fe self-diffusion, where all Γ_i take the same value, this gives $\Delta S_c = -0.32 k_B$. Likewise, when $\min(\Delta H_{\mathrm{mig},3}, \Delta H_{\mathrm{mig},3'}, \Delta H_{\mathrm{mig},3''}) < \Delta H_{\mathrm{mig},2}$, such as for Co, Ni, and W, Eq. (19) yields a temperature-independent value of f with $\Delta S_c \approx -0.32 k_B$. For the other impurity elements $\Delta S_c / k_B$ generally takes small positive values, in the neighborhood of unity, except for Ge, Zn, and Ca where $\Delta S_c / k_B \approx 2$.

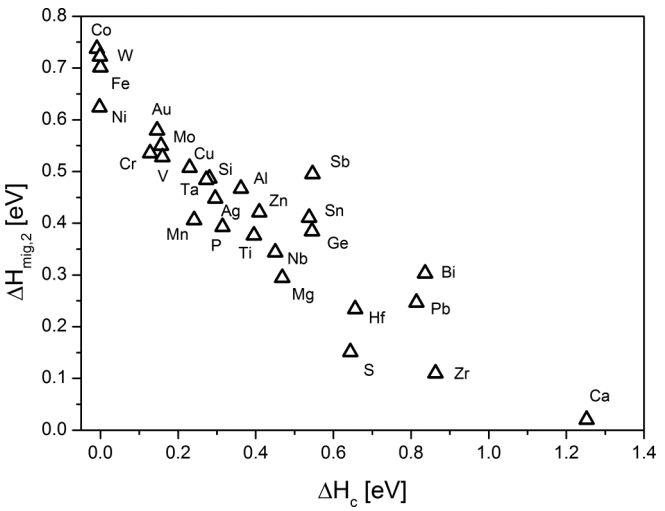

FIG. 7. ΔH_c from Eq. (20) as a function of $\Delta H_{\mathrm{mig},2}$.

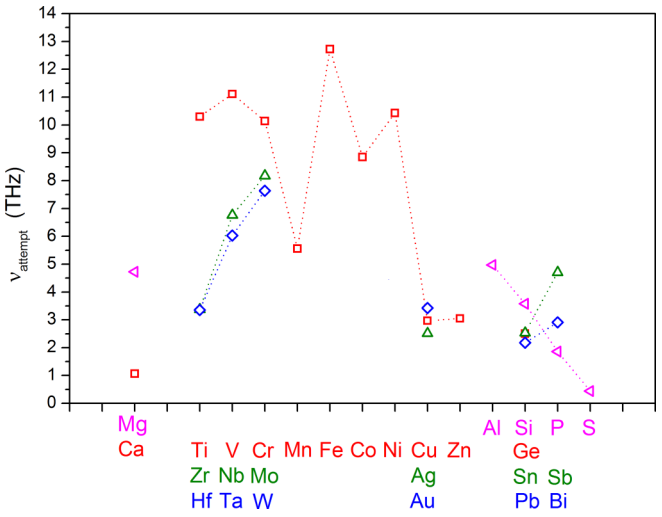

FIG. 8. The attempt frequencies for an impurity jump in iron calculated with Eq. (13), arranged by row and column of the periodic system: row 3 of the periodic system (purple triangles), row 4 of the periodic system (red squares), row 5 of the periodic system (green triangles), and row 6 of the periodic system (blue diamonds). Dashed lines, between neighboring impurities, are guides to the eyes only.

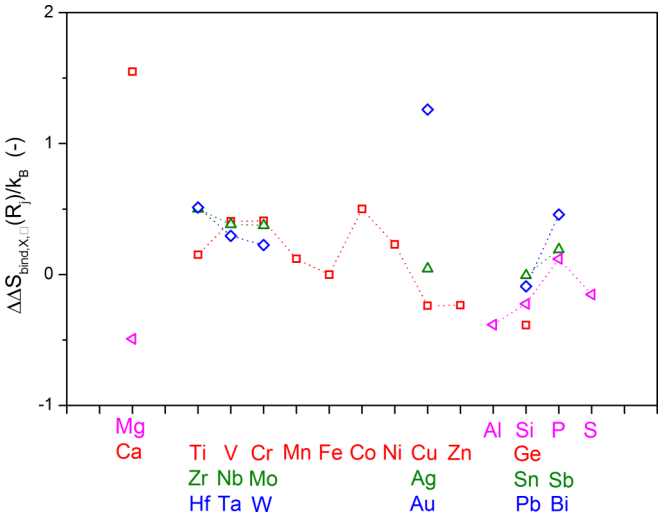

FIG. 9. The impurity-vacancy binding entropy in units of k_B, arranged by row and column of the periodic system: row 3 of the periodic system (purple triangles), row 4 of the periodic system (red squares), row 5 of the periodic system (green triangles), and row 6 of the periodic system (blue diamonds). Dashed lines, between neighboring impurities, are guides to the eyes only.

Recently, a more accurate expression for the correlation factor has been derived [61] where the jump rate between the second and fourth impurity atom neighbors is not equated to the bulk jump rate. Use of this equation did not yield any significant changes in our qualitative or quantitative results.

D. Diffusivities

For the calculation of diffusivities of impurities in iron, we examine first the parameters for the fully FM state as given by Eqs. (24) and (25). The element-specific terms in Eq. (25) are $\tilde{\nu}_2$, ΔS_c, and $\Delta\Delta S_{\text{bind},X\square}(\mathbf{R}_1)$, the other factors being independent of impurity species.

The effective attempt frequency for the diffusing species, $\tilde{\nu}_2$, has been computed using Eq. (13) (see Fig. 8, and Table II of the Supplemental Material [91]). Table II shows a number of remarkable results: For the $3d$ TM impurities attempt frequencies are generally high, with a remarkable dip for Mn in the middle of the series. The early $4d$ and $5d$ TM impurities are rather similar and have markedly lower attempt frequencies than the corresponding $3d$ TM impurities. The late TMs, Cu, Ag, and Au, all have rather similar attempt frequencies, in spite of their significant differences in atomic mass. Both the described tendencies and numerical values agree well with those found by Messina *et al.* [61]. Our frequencies are typically about 10% higher than those reported previously [61], which may be related to our somewhat smaller bcc lattice parameter. Given a typical temperature of 1000 K, a 10% error in the attempt frequency gives the same deviation in the computed diffusivity as an error in the diffusion activation energy of 8 meV. Concerning tendencies for frequencies of non-TM impurities, the rather low values stand out. These elements, such as Ca, Mg, Zn, Al, Si, Ge, Sn, Pb, P, Sb, and Bi all fall in the range of 1–5 THz, except S at 0.44 THz. Non-TM elements have lower frequencies as further down in the same column of the periodic system, as is seen in the comparison Mg-Ca, Si-Ge-Sn-Pb, and Sb-Bi. The $3p$ series Al-S also shows a marked decrease of frequencies as the number of p electrons increases, with a value of about 5 THz for Al and a very low value of 0.44 THz for S. We also applied a Meyer-Neldel fit to attempt frequency $\Delta H_{\text{mig},2}$. As before [61], the fit to the $3d$ TMs is very poor, but the fit to $3p$ elements [Al-S] also does not yield a physically significant result [99]. For the $3p$ elements an exponent of 0.507 and a Meyer-Neldel energy of 0.014 eV, as well as a reference frequency ν_0 of 0.01 THz, is found. These parameters differ strongly from what has been found for the $4d$ and $5d$ TM impurities [61], and appear to be closer to other analyses [100,101]. However, an alternate Meyer-Neldel analysis of the computed $\log(D_0)$ versus $\Delta H_{\text{mig},2}$ values does not yield a significant correlation because the D_0 are similar for all impurity elements considered. Therefore, the Meyer-Neldel analysis does not appear particularly useful for substitutional impurity diffusion in bcc iron.

The vibrational impurity-vacancy binding entropy, $\Delta\Delta S_{\text{bind},X\square}(\mathbf{R}_1)$, ranges from about -0.5 to $+1.5k_B$ (Fig. 9). The largest value is reached for Ca, and the smallest for Mg. For TM, values of about $+0.5k_B$ are common, while for non-TM, lower values predominate. Our data did not allow us to recognize any clear trends. Meyer-Neldel type correlations between $\Delta\Delta S_{\text{bind},X\square}(\mathbf{R}_1)$ and $\Delta H_{\text{mig},2}$ or Q_{FM} are not significant, reinforcing our conclusion that a Meyer-Neldel analysis is not particularly revealing.

The element-specific terms in Eq. (24), $\Delta H_{\text{bind},X\square}(\mathbf{R}_1)$, $\Delta H_{\text{mig},2}$, and ΔH_c have all been discussed above already, so that here we examine Q_{FM}. The activation energy for diffusion ranges from about 2 to 3 eV (Fig. 10), with most TM impurities within the range of 2.4–2.8 eV. This is in marked contrast to activation energies for substitutional impurity diffusion in metals such as Al [50] or Mg [51,52]. The activation energy

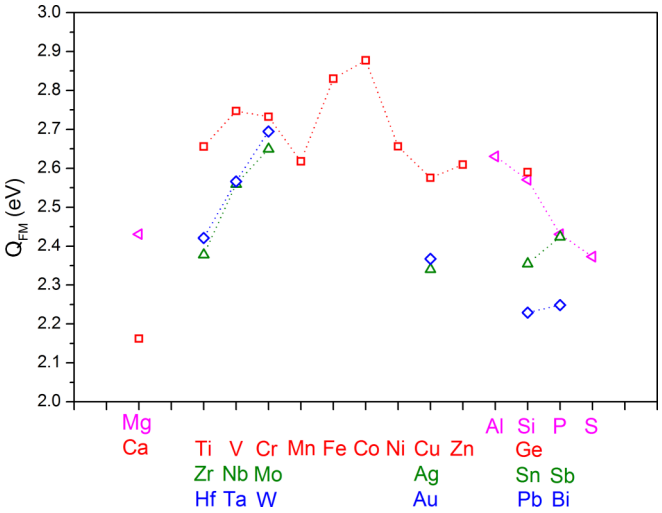

FIG. 10. PW91 total activation energies in a fully ferromagnetic state of impurity elements, arranged by row and column of the periodic system: row 3 of the periodic system (purple triangles), row 4 of the periodic system (red squares), row 5 of the periodic system (green triangles), and row 6 of the periodic system (blue diamonds). Dashed lines, between neighboring impurities, are guides to the eyes only.

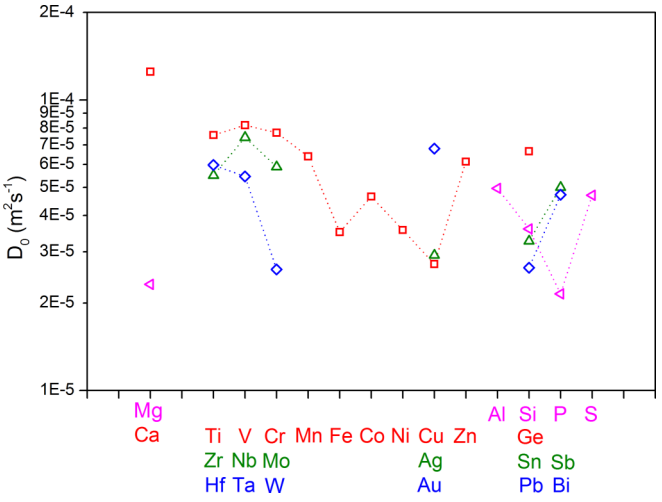

FIG. 11. Prefactors to diffusion, calculated with Eq. (25) are arranged by row and column of the periodic system: row 3 of the periodic system (purple triangles), row 4 of the periodic system (red squares), row 5 of the periodic system (green triangles), and row 6 of the periodic system (blue diamonds). Dashed lines, between neighboring impurities, are guides to the eyes only.

for TM impurities in aluminum can be twice that of aluminum self-diffusion while non-TM impurities often have activation energies which are very similar to that of the host [50,102]. The activation energies for the p-type elements in bcc iron show some interesting trends. The $3p$ impurities, Al-Si-P-S, display a monotonic decreasing diffusion activation energy in bcc Fe as the number of p electrons is increased. Along the columns of the periodic table too, a tendency is apparent where elements of the lower rows feature lower activation energies than those of the upper rows; Si-Ge-Sn-Pb and P-Sb-Bi. This tendency is already recognizable in the vacancy-impurity binding enthalpy and also in the impurity nearest-neighbor migration enthalpy. Increasing p-electron count strengthens the pd hybridization and thereby makes the vacancy-impurity binding increasingly less favorable. Furthermore, the loss of a number of nearest neighbors in the transition state is energetically less costly for a more covalently bonded element than for a metallically bonded element. Therefore the migration energy is lowered as the p-electron count increases. Of course, impurities further down a given column in the periodic system with their increased atomic size relax more toward the vacancy position, and have p bands that are wider and better aligned with the iron d bands to give a further decrease in migration energies. The element specific diffusion prefactors D_0 (see Fig. 11) are all within an order of magnitude of one another. There is no discernible trend with element size or with position in the period system.

A comparison of the computed impurity diffusivities with experimental data as a function of temperature requires consideration of the effect of magnetic (dis)ordering. The paramagnetic activation barrier has been computed in pure iron by Ding *et al.* [73] via the spin-wave method [74]. This provides a description of pure iron paramagnetic diffusion; however, to apply it for all impurity elements would not be trivial. Fortunately, the results [73] strongly resemble that of the semiempirical Girifalco model [64] so that we will be using that method here, just as was done in most diffusivity studies with regard to bcc iron so far. Our detailed review of experimental impurity diffusivities above and below the Curie temperature [68] has revealed that the Girifalco α parameter [see Eq. (2)] for all impurities in the dilute limit can be reasonably chosen as $\alpha = 0.10$, with the exception of iron self-diffusion for which $\alpha = 0.16$ is in better agreement with the majority of experimental data.

The diffusivities of impurity elements in bcc iron calculated with PW91 agree well with the experimental results. The diffusivities of impurities in bcc iron are close together experimentally, which is reflected in the calculated results. The greatest deviation from between calculated and experimental results are in overestimating the diffusivities of Mn, Zn, Nb, Ta, and Au in bcc iron (see Fig. 12). For those elements that are not compared to experiments the diffusivities are presented in Fig. 13. Notably high diffusivities are found for Pb and Ca in bcc iron; this coincides with a very low solubility. The reason for this seems to be underestimated activation barriers, which is especially seen in the low-temperature deviation between the PW91 line and experimentally measured points. In other cases there is an overestimation of diffusivity as calculated by PW91. The reason for this seems similar, but opposite, in the way that there is discrepancy in the slope of the diffusivities.

The agreement with measured diffusivities is most cases very good, especially considering the discrepancy between various experimental data sets of dilute impurity diffusion. The methodology presented here provides reliable results for the determination of diffusivity in bcc iron.

The results for the vacancy binding energies, migration barriers, and diffusivities are compared (in the Supplemental Material [91]) to the calculated results of [54,56,57,60,61,88,90,98,103,104] for which migration bar-

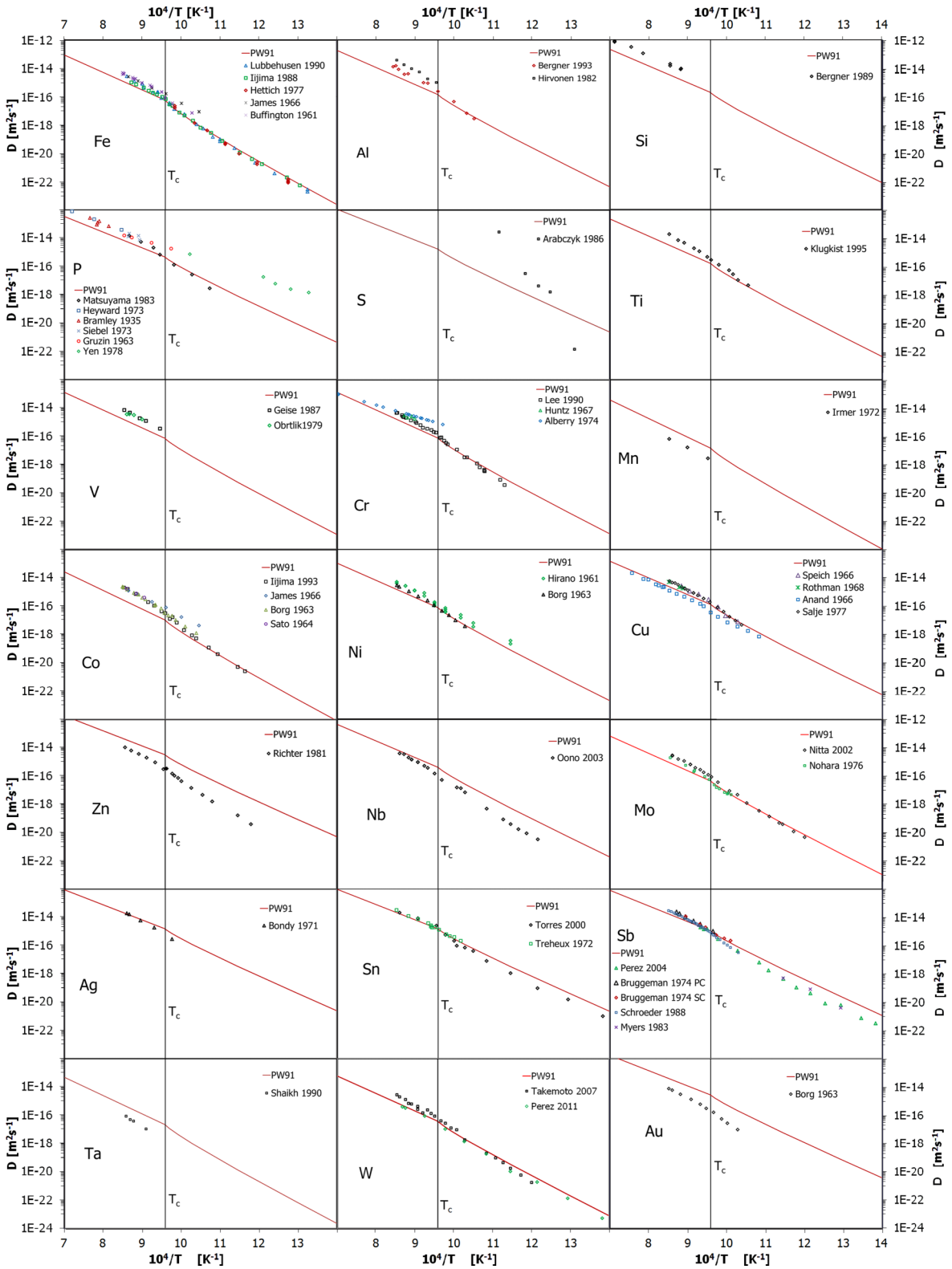

FIG. 12. The diffusivity as calculated with the PW91 xc functional (red lines), compared to experimental data of Fe [3–7] self-diffusion and dilute impurity diffusion of Al [8,9], Si [10], P [11–16], S [17], Ti [18], V [19,20], Cr [21–23], Mn [24], Co [2,6,25,26], Ni [2,27], Cu [28–31], Zn [32], Nb [33], Mo [34,35], Ag [36], Sn [37,38], Sb [39–42], Ta [43], W [44,45], and Au [2]. The Curie temperature (T_C) is indicated by a vertical black line in all panels.

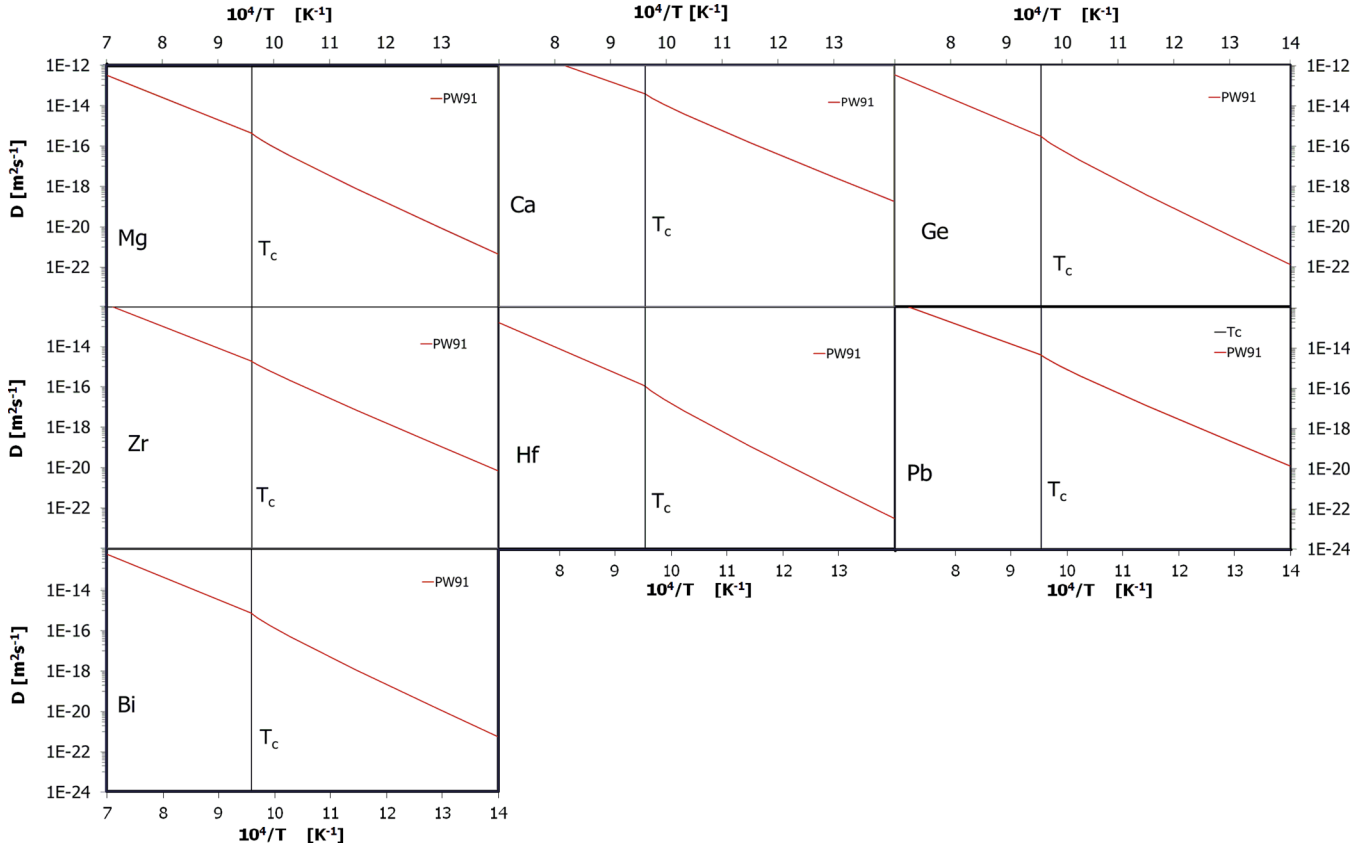

FIG. 13. The impurity diffusion of elements Mg, Ca, Ge, Zr, Hf, Pb, and Bi in bcc iron. Diffusivities as calculated with the PW91 xc functional (red lines). The Curie temperature (T_C) is indicated by a vertical black line in all panels.

riers were found to be very similar in all cases. Differences are found in vacancy formation energies, which is very sensitive to the type of exchange-correlation functional.

One general trend captured very well in the calculations is that all diffusivities are very close together for impurities in bcc iron. This indicates a similar mechanism and as well a rate of diffusion which is determined by the self-diffusion of vacancies in the iron matrix. The trend that the activation energy for diffusion is dependent on the column of the periodic system is captured both by the diffusivity calculations and the comparison to experiments. This makes the trends captured by these calculations very useful to predict the diffusivities of those elements whose diffusivities have not yet been determined experimentally.

V. CONCLUSIONS

Diffusivities of a large number of impurities in bcc iron have been calculated by means of first-principle methods. The selection of the elements of the periodic table gives a good overview of all single-vacancy diffusing elements. The magnitude of the vacancy formation energies is highly dependent on the chosen exchange-correlation functional, unlike the magnitude of migration barriers.

The magnitudes of the nearest-neighbor barriers, vacancy formation, and binding energies are correlated to the position of the element in the periodic system, with low values on each end of the columns of the periodic system. This is compensated by the effective enthalpy barrier caused by the temperature dependence of the correlation factor. The diffusivity of any single-vacancy diffusing element in bcc iron is dominated by the diffusivity of a vacancy through the host. All single-vacancy diffusing elements are expected to follow the same trends that the calculated elements do. The activation energies for diffusion are presented in Fig. 10. The nearest-neighbor barrier for the elements strontium, barium, lanthanum, and cerium is so low, that it likely does not diffuse through the single-vacancy mechanism. It is more plausible that they form an impurity-vacancy complex which requires another vacancy to diffuse.

All elements except Co, Mn, and Ta show greater diffusivity than iron self-diffusion, which is confirmed by the experimental data. The other elements show good agreement with experiments. In bcc iron most substitutional elements diffuse within one order of magnitude faster than bcc iron self-diffusion. Some faster diffusing elements are Au, Pb, and Ca, with Pb diffusing two orders of magnitude faster than Fe. For the other diffusivities, each impurity element in bcc iron seems to be limited by the self-diffusivity of vacancies in iron.

When considering the position of the element in the periodic table, trends in the the rates of diffusivities of impurity elements in bcc iron can be observed, with fast diffusing elements at the columns furthest away from Fe and elements in columns close to Fe with diffusivities similar to Fe self-diffusivity. Less important seems to be the row of the periodic system.

ACKNOWLEDGMENTS

The authors thank Professor Ekkes Brück, Professor Sybrand van der Zwaag, Dr. Fritz Körmann, Dr. Shasha Zhang, and Haixing Fang for discussions. The authors gratefully acknowledge financial support from the Rijksdienst voor Ondernemend Nederland (IOP program for Self Healing Materials SHM012011).

[1] G. Neumann and C. Tuijn, in *Self-Diffusion and Impurity Diffussion in Pure Metals*, 1st ed. (Elsevier, New York, 2008), p. 121.
[2] R. J. Borg and D. Y. F. Lai, Acta Metall. **11**, 861 (1963).
[3] M. Lübbehusen and H. Mehrer, Acta Metall. Mater. **38**, 283 (1990).
[4] Y. Iijima and K. Hirano, Acta Metall. **36**, 2811 (1988).
[5] G. Hettich, H. Mehrer, and K. Maier, Scr. Metall. **11**, 795 (1977).
[6] D. W. James and G. M. Leak, Philos. Mag. **14**, 701 (1966).
[7] F. S. Buffington, K. Hirano, and M. Cohen, Acta Metall. **9**, 434 (1961).
[8] D. Bergner and Y. Khaddour, Defect Diffus. Forum **95-98**, 709 (1993).
[9] J. Hirvonen and J. Räisänen, J. Appl. Phys. **53**, 3314 (1982).
[10] D. Bergner, Y. Khaddour, and S. Lörx, Defect Diffus. Forum **66-69**, 1407 (1990).
[11] T. Matsuyama, H. Hosokawa, and H. Suto, Trans. Jpn. Inst. Met. **24**, 589 (1983).
[12] T. Heyward and J. I. Goldstein, Metall. Trans. **4**, 2335 (1973).
[13] A. Bramley, F. W. Haywood, A. T. Cooper, and J. T. Watts, Trans. Faraday Soc. **31**, 707 (1934).
[14] G. Siebel, C. R. Acad. Sci. **256**, 4661 (1963).
[15] P. L. Gruzin and V. V. Mural, Fiz. Met. Met. **16**, 551 (1963).
[16] A. C. Yen, W. R. Graham, and G. R. Belton, Metall. Trans. A **9**, 31 (1978).
[17] W. Arabczyk, M. Militzer, H.-J. Müssig, and J. Wieting, Scr. Metall. **20**, 1549 (1986).
[18] P. Klugkist and C. Herzig, Phys. Status Solidi A **148**, 413 (1995).
[19] J. Geise and C. Herzig, Z. Metallkd. **78**, 291 (1987).
[20] K. Obrtlík and J. Kučera, Phys. Status Solidi A **53**, 589 (1979).
[21] C.-G. Lee, Y. Iijima, T. Hiratani, and K. Hirano, Mater. Trans., JIM **31**, 255 (1990).
[22] A. M. Huntz, M. Aucouturier, and P. Lacombe, C. R. Acad. Sci. Paris, Ser. C **265**, 554 (1967).
[23] P. J. Alberry and C. W. Haworth, Met. Sci. J. **8**, 407 (1974).
[24] V. Irmer and M. Feller-Kniepmeier, J. Phys. Chem. Solids **33**, 2141 (1972).
[25] Y. Iijima, K. Kimura, C.-G. Lee, and K. Hirano, Mater. Trans., JIM **34**, 20 (1993).
[26] K. Sato, Trans. Jpn. Inst. Met. **5**, 91 (1964).
[27] K. Hirano, M. Cohen, and B. Averbach, Acta Metall. **9**, 440 (1961).
[28] G. Speich, J. Gula, and R. M. Fisher, in *The Electron Microprobe*, edited by D. W. T. D. McKinley and K. F. Heinrich (Wiley, New York, 1966), p. 525.
[29] S. Rothman, N. Peterson, C. Walter, and L. Nowicki, J. Appl. Phys. **39**, 5041 (1968).
[30] M. S. Anand and R. P. Agarwala, J. Appl. Phys. **37**, 4248 (1966).
[31] G. Salje and M. Feller-Kniepmeier, J. Appl. Phys. **48**, 1833 (1977).
[32] I. Richter, Phys. Status Solidi A **68**, 289 (1981).
[33] N. Oono, H. Nitta, and Y. Iijima, Mater. Trans. **44**, 2078 (2003).
[34] H. Nitta, T. Yamamoto, R. Kanno, K. Takasawa, T. Iida, Y. Yamazaki, S. Ogu, and Y. Iijima, Acta Mater. **50**, 4117 (2002).
[35] K. Nohara and K. Hirano, J. Jpn. Inst. Met. **40**, 1053 (1976).
[36] A. Bondy and V. Levy, C. R. Acad. Sci. Paris Ser. C **272**, 19 (1971).
[37] D. N. Torres, R. A. Perez, and F. Dyment, Acta Mater. **48**, 2925 (2000).
[38] D. Treheux, D. Marchive, J. Delagrange, and P. Guiraldenq, C. R. Acad. Sci. Ser. C **274**, 1260 (1972).
[39] R. A. Pérez, D. N. Torres, and F. Dyment, Appl. Phys. A **81**, 787 (2005).
[40] G. A. Bruggeman and J. A. Roberts, Metall. Trans. A **6**, 755 (1975).
[41] A. Schröder and M. Feller-Kniepmeier, Phys. Status Solidi A **110**, 107 (1988).
[42] S. Myers, *Nontraditional Methods in Diffusion*, edited by G. E. Murch, H. K. Birnbaum, and J. R. Cost (Metallurgical Society of AIME, New York, NY, 1984), p. 137.
[43] Q. A. Shaikh, Mater. Sci. Technol. **6**, 1177 (1990).
[44] S. Takemoto, H. Nitta, Y. Iijima, and Y. Yamazaki, Philos. Mag. **87**, 1619 (2007).
[45] R. A. Pérez and D. N. Torres, Appl. Phys. A **104**, 329 (2011).
[46] B. Medasani, M. Haranczyk, A. Canning, and M. Asta, Comput. Mater. Sci. **101**, 96 (2015).
[47] T. Hickel, B. Grabowski, F. Körmann, and J. Neugebauer, J. Phys.: Condens. Matter **24**, 053202 (2012).
[48] J. Janßen, N. Gunkelmann, and H. M. Urbassek, Philos. Mag. **96**, 1448 (2016).
[49] G. Steinle-Neumann, L. Stixrude, and R. E. Cohen, Phys. Rev. B **60**, 791 (1999).
[50] D. Simonovic and M. H. F. Sluiter, Phys. Rev. B **79**, 054304 (2009).
[51] L. Huber, I. Elfimov, J. Rottler, and M. Militzer, Phys. Rev. B **85**, 144301 (2012).
[52] B. C. Zhou, S. L. Shang, Y. Wang, and Z. K. Liu, Data Br. **5**, 900 (2015).
[53] M. Krčmar, C. L. Fu, A. Janotti, and R. C. Reed, Acta Mater. **53**, 2369 (2005).
[54] S. Choudhury, L. Barnard, J. D. Tucker, T. R. Allen, B. D. Wirth, M. Asta, and D. Morgan, J. Nucl. Mater. **411**, 1 (2011).
[55] J. D. Tucker, R. Najafabadi, T. R. Allen, and D. Morgan, J. Nucl. Mater. **405**, 216 (2010).
[56] C. Domain, J. Nucl. Mater. **351**, 1 (2006).
[57] S. Huang, D. L. Worthington, M. Asta, V. Ozolins, G. Ghosh, and P. K. Liaw, Acta Mater. **58**, 1982 (2010).

[58] E. Vincent, C. S. Becquart, and C. Domain, Nucl. Instrum. Methods Phys. Res., Sect. B **228**, 137 (2005).
[59] C. S. Becquart and C. Domain, Nucl. Instrum. Methods Phys. Res., Sect. B **202**, 44 (2003).
[60] H. Ding, S. Huang, G. Ghosh, P. K. Liaw, and M. Asta, Scr. Mater. **67**, 732 (2012).
[61] L. Messina, M. Nastar, N. Sandberg, and P. Olsson, Phys. Rev. B **93**, 184302 (2016).
[62] Y. Iijima, J. Phase Equilibria Diffus. **26**, 466 (2005).
[63] L. Girifalco, J. Phys. Chem. Solids **25**, 323 (1964).
[64] L. Ruch, D. R. Sain, H. L. Yeh, and L. A. Girifalco, J. Phys. Chem. Solids **37**, 649 (1976).
[65] C. Varvenne, F. Bruneval, M. C. Marinica, and E. Clouet, Phys. Rev. B **88**, 134102 (2013).
[66] D. C. Wallace, Thermodynamics of Crystals, Dover Books on Physics (Dover, New York, 1998), pp. 180–183.
[67] A. S. Arrott and B. Heinrich, J. Appl. Phys. **52**, 2113 (1981).
[68] C. D. Versteylen, N. H. van Dijk, and M. H. F. Sluiter (unpublished).
[69] G. H. Vineyard, J. Phys. Chem. Solids **3**, 121 (1957).
[70] A. D. Le Claire, Philos. Mag. **21**, 819 (1970).
[71] M. J. Jones and A. D. Le Claire, Philos. Mag. **26**, 1191 (1972).
[72] J. Neuhaus, W. Petry, and A. Krimmel, Phys. B: Condens. Matter **234-236**, 897 (1997).
[73] H. Ding, V. I. Razumovskiy, and M. Asta, Acta Mater. **70**, 130 (2014).
[74] A. V. Ruban and V. I. Razumovskiy, Phys. Rev. B **85**, 174407 (2012).
[75] F. Körmann, B. Grabowski, B. Dutta, T. Hickel, L. Mauger, B. Fultz, and J. Neugebauer, Phys. Rev. Lett. **113**, 165503 (2014).
[76] S. Baroni, S. De Gironcoli, A. Dal Corso, and P. Giannozzi, Rev. Mod. Phys. **73**, 515 (2001).
[77] G. Kresse and J. Furthmüller, Comput. Mater. Sci. **6**, 15 (1996).
[78] G. Kresse and J. Furthmüller, Phys. Rev. B **54**, 11169 (1996).
[79] P. E. Blöchl, Phys. Rev. B **50**, 17953 (1994).
[80] G. Kresse and D. Joubert, Phys. Rev. B **59**, 1758 (1999).
[81] G. Henkelman and H. Jonsson, J. Chem. Phys. **113**, 9978 (2000).
[82] J. P. Perdew and Y. Wang, Phys. Rev. B **45**, 13244 (1992).
[83] J. P. Perdew, J. A. Chevary, S. H. Vosko, K. A. Jackson, M. R. Pederson, D. J. Singh, and C. Fiolhais, Phys. Rev. B **46**, 6671 (1992).
[84] J. P. Perdew, A. Ruzsinszky, G. I. Csonka, O. A. Vydrov, G. E. Scuseria, L. A. Constantin, X. Zhou, and K. Burke, Phys. Rev. Lett. **100**, 136406 (2008).
[85] P. Haas, F. Tran, and P. Blaha, Phys. Rev. B **79**, 085104 (2009).
[86] R. Nazarov, T. Hickel, and J. Neugebauer, Phys. Rev. B **85**, 144118 (2012).
[87] Y. Jiang, J. R. Smith, and G. R. Odette, Phys. Rev. B **79**, 064103 (2009).
[88] C. Zhang, J. Fu, R. Li, P. Zhang, J. Zhao, and C. Dong, J. Nucl. Mater. **455**, 354 (2014).
[89] D. Murali, M. Posselt, and M. Schiwarth, Phys. Rev. B **92**, 064103 (2015).
[90] X. Gao, H. Ren, C. Li, H. Wang, Y. Ji, and H. Tan, J. Alloys Compd. **663**, 316 (2016).
[91] See Supplemental Material at http://link.aps.org/supplemental/10.1103/PhysRevB.96.094105 for tables containing the enthalpies and entropies of defect formation and the jump barriers.
[92] A. Glensk, B. Grabowski, T. Hickel, and J. Neugebauer, Phys. Rev. X **4**, 011018 (2014).
[93] T. Tiedje, J. M. Cebulka, D. L. Morel, and B. Abeles, Phys. Rev. Lett. **46**, 1425 (1981).
[94] G. Lucas and R. Schäublin, Nucl. Instrum. Methods Phys. Res., Sect. B **267**, 3009 (2009).
[95] A. T. Dinsdale, Calphad **15**, 317 (1991).
[96] T. Ohnuma, N. Soneda, and M. Iwasawa, Acta Mater. **57**, 5947 (2009).
[97] P. Olsson, T. P. C. Klaver, and C. Domain, Phys. Rev. B **81**, 054102 (2010).
[98] D. Murali, B. K. Panigrahi, M. C. Valsakumar, and C. S. Sundar, J. Nucl. Mater. **419**, 208 (2011).
[99] A fit of three parameters to just four data points is questionable in any case.
[100] G. Boisvert and L. J. Lewis, Phys. Rev. B **54**, 2880 (1996).
[101] M. C. Marinica, C. Barreteau, D. Spanjaard, and M. C. Desjonquères, Phys. Rev. B **72**, 115402 (2005).
[102] T. Marumo, S. Fujikawa, and K. Hirano, J. Jpn. Inst. Light Met. **23**, 17 (1973).
[103] A. Claisse and P. Olsson, Nucl. Instrum. Methods Phys. Res., Sect. B **303**, 18 (2013).
[104] E. Vincent, C. S. Becquart, and C. Domain, Nucl. Instrum. Methods Phys. Res., Sect. B **255**, 78 (2007).
[105] L. Messina, M. Nastar, T. Garnier, C. Domain, and P. Olsson, Phys. Rev. B **90**, 104203 (2014).